JACS
JOURNAL OF THE AMERICAN CHEMICAL SOCIETY
Article
pubs.acs.org/JACS

Negative Differential Resistance by Molecular Resonant Tunneling between Neutral Tribenzosubporphine Anchored to a Au(111) Surface and Tribenzosubporphine Cation Adsorbed on to a Tungsten Tip

Yutaka Majima,*[,†,‡,§] Daisuke Ogawa,[†,‡] Masachika Iwamoto,[†,‡] Yasuo Azuma,[†,‡] Eiji Tsurumaki,[∥] and Atsuhiro Osuka*[,∥]

[†]Materials and Structures Laboratory, Tokyo Institute of Technology, Yokohama 226-8503, Japan
[‡]CREST, Japan Science and Technology Agency (JST), Yokohama 226-8503, Japan
[§]Department of Printed Electronics Engineering, Sunchon National University, Sunchon 540-742, Korea
[∥]Department of Chemistry, Graduate School of Science, Kyoto University, Sakyo-ku, Kyoto 606-8502, Japan

Supporting Information

ABSTRACT: Tribenzosubporphyrins are boron(III)-chelated triangular bowl-shaped ring-contracted porphyrins that possess a 14π-aromatic circuit. Their flat molecular shapes and discrete molecular orbital diagrams make them ideal for observation by scanning tunneling microscopy (STM). Expanding their applications toward single molecule-based devices requires a fundamental knowledge of single molecular conductance between tribenzosubporphines and the STM metal tip. We utilized a tungsten (W) STM tip to investigate the electronic properties of B-(5-mercaptopentoxy)tribenzosubporphine **1** at the single molecular level. B-(5-mercaptopentoxy)-tribenzosubporphine **1** was anchored to the Au(111) surface via reaction with 1-heptanethiol linkers that were preorganized as a self-assembled monolayer (C7S SAM) on the Au(111) substrate. This arrangement ensured that **1** was electronically decoupled from the metal surface. Differential conductance ($dI/dV - V$) measurements with the bare W tip exhibited a broad gap region of low conductance and three distinct responses at 2.4,−1.3, and −2.1 V. Bias-voltage-dependent STM imaging of **1** at 65 K displayed a triangle shape at $-2.1 < V < -1.3$ V and a circle shape at $V < -2.1$ V, reflecting its HOMO and HOMO−1, respectively. In addition, different conductance behaviors were reproducibly observed, which has been ascribed to the adsorption of a tribenzosubporphine-cation on the W tip. When using a W tip doped with preadsorbed tribenzosubporphine-cation, negative differential resistance (NDR) phenomena were clearly observed in a reproducible manner with a peak-to-valley ratio of 2.6, a value confirmed by spatial mapping conductance measurements. Collectively, the observed NDR phenomena have been attributed to effective molecular resonant tunneling between a neutral tribenzosubporphine anchored to the metal surface and a tribenzosubporphine cation adsorbed on a W tip.

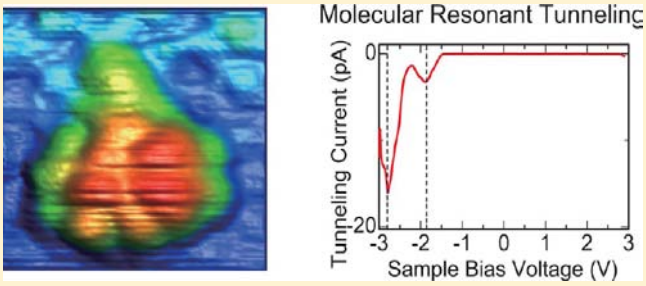

INTRODUCTION

Prior to the construction of molecular electronic devices that contain multiple components, it is necessary to understand the electrical properties of individual molecules. π-Conjugated molecules have played a central role in the construction of molecular electronic devices.[1−10] Negative differential resistance (NDR) behavior, which is an initial rise followed by a decrease in current with increasing voltage, is a phenomena that is extensively used to study the operational capacity of molecular devices.[11−13] NDR phenomena have been demonstrated by using π-conjugated molecules such as oligo(phenylene-ethynylene),[11−19] fullerene,[20−23] phthalocyanines,[24] and porphyrins.[25,26] While various mechanisms have been proposed for NDR, the most important mechanism is a molecular-origin resonant tunneling diode (RTD). In conventional RTD with compound semiconductors, there is a quantum well between two tunnel barriers with doped contacts on either side to form reservoirs of electrons.[27] When a voltage is applied, a current can only flow when electrons can tunnel through the sub-band state in the quantum well. For NDR behavior, these sub-bands have to constitute discrete energy levels. Therefore, π-conjugated molecules with discrete energy levels originating from molecular orbitals can be used as quantum wells in molecular RTD.

Tribenzosubporphines, the first reported case of a subporphyrins in 2006,[28] constitute an interesting class of π-conjugated molecules in light of their 14π-aromatic circuits,

Received: May 14, 2013
Published: September 11, 2013

   dx.doi.org/10.1021/ja404512w | J. Am. Chem. Soc. 2013, 135, 14159−14166

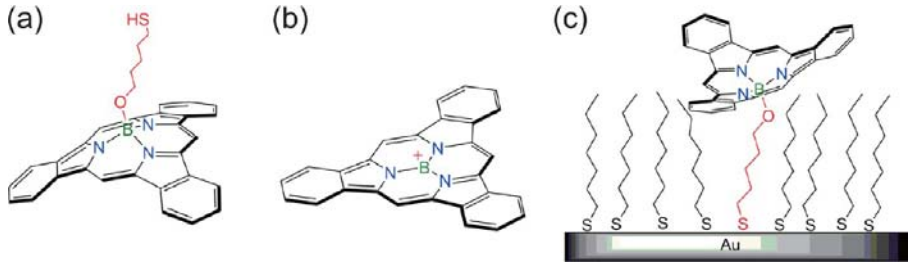

Figure 1. Molecular structures of (a) B-(5-mercaptopentoxy)tribenzosubporphine (**1**) and (b) B-tribenzosubporphine cation. (c) Schematic side view consisting of B-pentanethioloxy tribenzosubporphine:C7S mixed self-assembled monolayer (SAM)/Au(111).

triangular bowl-shaped structures, intense green fluorescence and nonlinear optical properties.[29,30] In addition, due to the lack of substituents at the *meso* position, tribenzosubporphines possess streamlined contours that are ideal for single molecular observation by STM. Density functional theory (DFT) calculations reveal that tribenzosubporphines have molecular orbital diagrams with discrete energy levels of frontier orbitals such as HOMO−1, HOMO, and nearly generate LUMO, reflecting their compact aromatic system. These features are considered to be ideal for detection of RTD phenomena.

Molecular-resolution STM and scanning tunneling spectroscopy (STS) are powerful tools for probing the electrical properties of individual molecules, providing us with vital information on adsorption geometry, intermolecular patterns and local conductivity of single molecules.[23,24,26,31] These characteristics allow us to understand the function of single molecules and the mechanism of how they operate which in turn allow us to intelligently design more complicated multicomponent architectures.

This work reported here demonstrates molecular electronic device operations of tribenzosubporphine in a single molecular level by combination of STM and STS. Importantly, NDR phenomena have been clearly observed during spatial mapping conductance measurements, which have been attributed to molecular resonant tunneling between a neutral tribenzosubporphine anchored to the metal surface and a trizenbosubporphine cation adsorbed on a W tip.

EXPERIMENTAL SECTION

B-Methoxytribenzosubporphine was prepared by the condensation of 2-(3-oxo-2,3-dihydro-1H-isoindol-1-yl)acetic acid by following previously reported method,[28] and was converted to B-(5-mercaptopentoxy)tribenzosubporphine **1** by heating in the presence of 5-mercaptopentanol in CH_2Cl_2 (Figure 1a) 1-Heptanethiol (C7S) of reagent grade quality was purchased from Wako Chemicals Ltd. and used without further purification. The Au(111) substrate was fabricated by thermal evaporation of gold onto freshly cleaved mica. Prior to gold evaporation, the mica substrates were held in a vacuum at 773 K for 4 h. The temperature was maintained at 773 K during gold evaporation, and postannealing was performed at 748 K for 1 h. The substrate was briefly flame-annealed and then quenched with ethanol to form an atomically flat Au(111) surface. This Au(111) substrate was immersed in a 1 mM solution of C7S in ethanol for 24 h and was rinsed with ethanol two times and dried in a pure N_2 flow to form the C7S SAM coated Au(111) substrate. The resulting substrate was then immersed in a 0.1 mM solution of **1** in acetonitrile for 3 h to form a substrate in which **1** was anchored to the Au(111) surface, being embedded in C7S SAM (Figure 1c). Importantly, **1** is electronically well decoupled from the Au(111) surface and probably floated on C7S SAM with its concave face directing upward. The rinsed sample was immediately introduced into a modified UHV-STM system with a base pressure below 3.0×10^{-8} Pa (UNISOKU). The STM images were measured by varying sample voltages (V) in a constant-current mode at 65 K. The STM tip was an electro-polished W probe. During STS measurements, the tip was held at a fixed position above the sample surface. The sample bias voltage is applied to the Au(111) substrate.

RESULTS AND DISCUSSION

Figure 2a−e shows STM images (2.5×2.5 nm^2) of a single molecule of **1** inserted in C7S SAM at various sample voltage with a set point current of −4 pA. A periodic structure behind **1** was due to the head part of C7S SAM. These STM images show a triangle-like structure. Bias-voltage dependence was

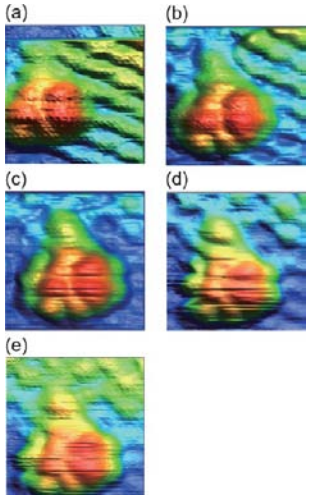

Figure 2. (a−e) STM images of single B-pentanethioloxy tribenzosubporphine inserted in C7S SAM under the sample bias voltage of −2.4,−2.2,−2.0,−1.8 and −1.6 V, respectively, at the set point current of −4 pA. STM image size is 2.5×2.5 nm^2.

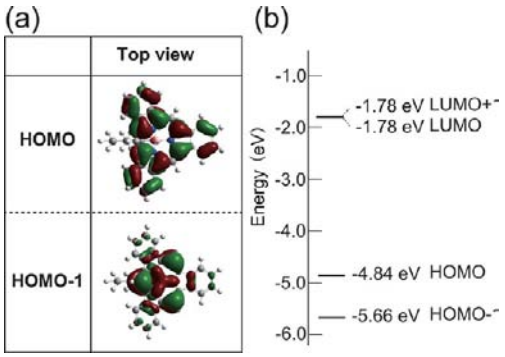

Figure 3. (a) Kohn−Sham molecular orbitals of B-pentanethioloxy tribenzosubporphine with isovalue of 0.02 e/A^3 at HOMO and HOMO−1, respectively. (b) Energy levels of calculated Kohn−Sham molecular orbitals.

dx.doi.org/10.1021/ja404512w | J. Am. Chem. Soc. 2013, 135, 14159−14166

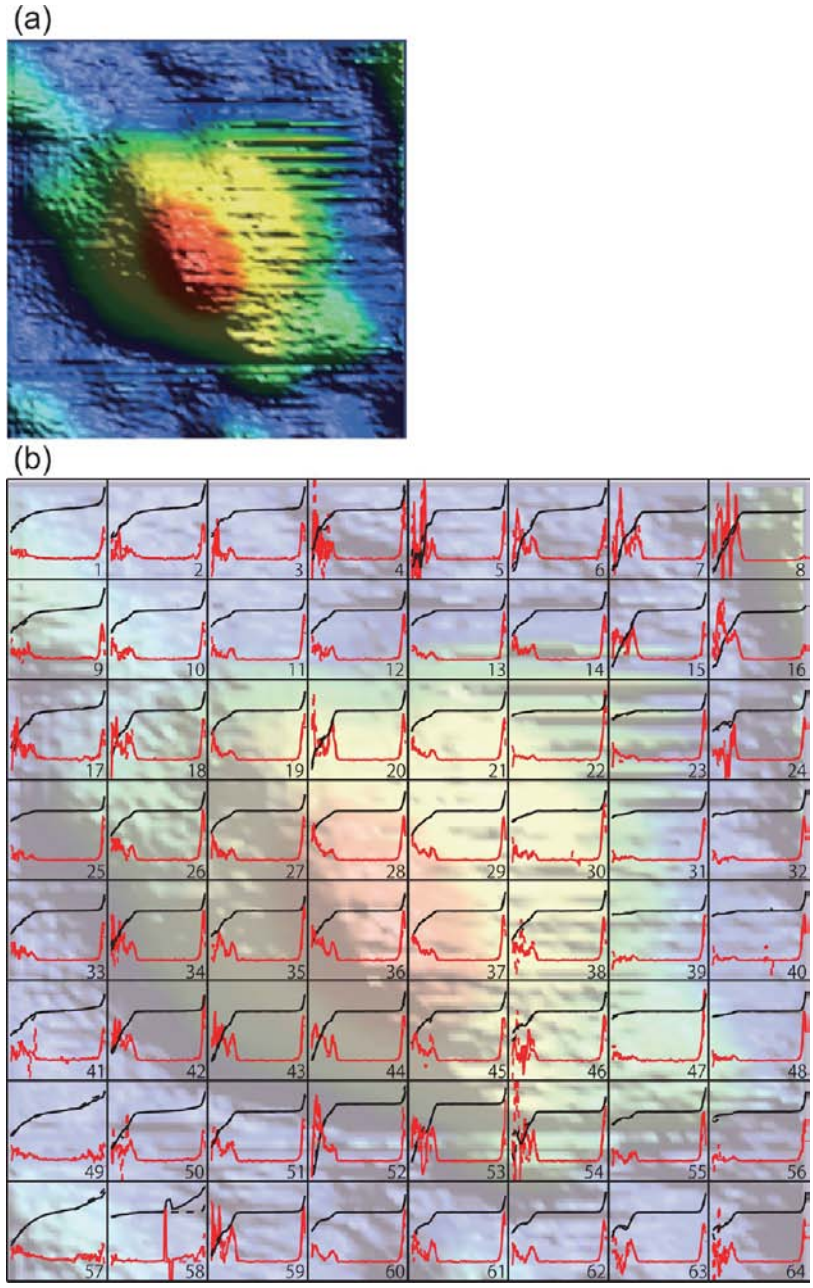

Figure 4. (a) STM image of B-pentanethioloxy tribenzosubporphine inserted in C7S SAM by bare W tip with 3 × 3 nm^2 at the sample bias voltage of −1.4 V and a set point current of −12 pA. (b) Spatial mapping of current−voltage (I−V, black lines) and differential conductance-voltage (dI/dV − V, red lines) characteristics at all the 8 × 8 divided parts of the STM image with consecutive bidirectional sample bias voltage sweeps from −2.5 to 2.5 V (solid line) and from 2.5 to −2.5 V (dashed line). The STM image of (a) is overlaid.

observed at the right side angle of **1**, that is, a valley structure was observed at low bias voltage region (∼−1.6 to −1.8 V), while a rounded fringe structure was observed at −2.2 V.

To demonstrate the Kohn−Sham molecular orbitals of **1**, we have carried out ab initio pseudopotential DFT calculations.[32,33] Geometry optimizations were carried out using the B3LYP functional and 6-31G (d) basis set with Gaussian 03.[34−36] Graphical presentations of the computational results were generated by using GaussView 4.1 (Gaussian Inc.). Figure 3a shows that calculated Kohn−Sham HOMO and HOMO−1 eigenvalues and orbitals of isolated **1**. It is important to note that the valley and rounded fringe structures agree with the Kohn−Sham molecular orbitals of HOMO and HOMO−1 of **1**. Figure 3b shows the energy levels of calculated Kohn−Sham molecular orbitals, which indicates that characteristically LUMO and LUMO+1 are nearly degenerate.[28]

Figure 4a shows an STM image (3 × 3 nm^2) of an individual molecule of **1** inserted in C7S SAM with the bare W tip at the sample bias voltage of −1.4 V and a set point current of −12 pA. In Figure 4b, current−voltage (I−V, black lines) and differential conductance-voltage (dI/dV − V, red lines) characteristics were measured at all the 8 × 8 divided parts of the STM image in Figure 4a with consecutive bidirectional sample bias voltage sweeps from −2.5 to 2.5 V (backward sweep, solid line) and from 2.5 to −2.5 V (forward sweep, dashed line). Spatial mapping STS is not easy and time-consuming but we employed this in order to reveal detailed molecular orbital features in a single molecular level.[37] Here it is

dx.doi.org/10.1021/ja404512w | J. Am. Chem. Soc. 2013, 135, 14159−14166

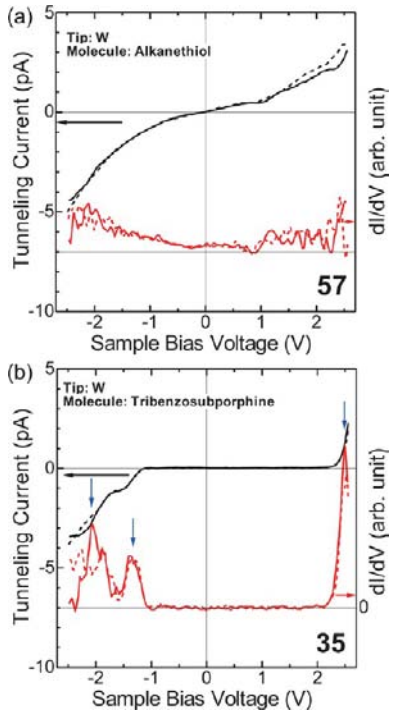

Figure 5. Representative $I-V$ and $dI/dV - V$ characteristics measured on (a) C7S SAM and (b) B-pentanethioloxy tribenzosubporphine with a bare W tip, which correspond the parts 57 and 35 of Figure 4b, respectively.

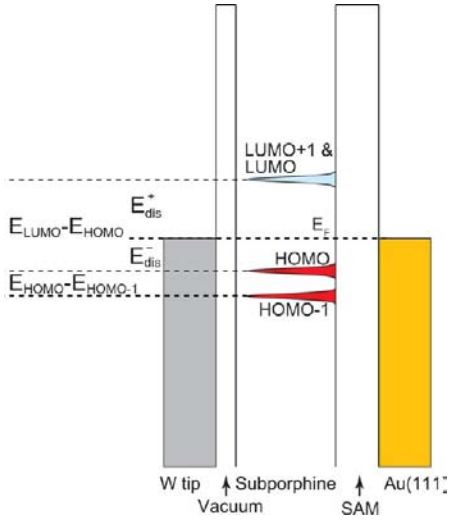

Figure 6. Energy diagrams of W tip/vacuum/B-pentanethioloxy tribenzosubporphine:C7S SAM/Au(111) structure.

important to note that the employed spacing area is relatively small as compared with the actual molecular size of tribenzosubporphine, which caused a complicated situation that $I-V$ and $dI/dV - V$ responses measured by STS do not necessarily reflect the molecular occupying area recorded by STM. Importantly, however, we have confirmed that the measurement results of backward sweeps agree well with those of forward sweeps for all of 64 parts, which assures the reliability of the measurement results of $I-V$ and $dI/dV - V$ curves.

The $I-V$ and $dI/dV - V$ characteristics are clearly different between **1**-detecting parts and **1**-free parts in a rough sense. Figure 5a and b shows the representative $I-V$ and $dI/dV - V$ characteristics of such two parts, that is, part 57 and part 35 designated in Figure 4b. Figure 5a shows low conductance in a wide range between 2.5 and −2.5 V without discernible dI/dV peak in accord with no electroactive material of C7S at part 57, while Figure 5b exhibits low-conductance in a range between 2 and −1 V but displays discrete dI/dV peaks at V = 2.4, −1.3, and −2.1 V, apparently via the availability of the conductance between the tip and the molecular orbitals of **1**. It notes that the $I-V$ and $dI/dV - V$ characteristics on parts of 16, 59 to 64 look similar to the data on part 35 (Figure 5b). These results suggest that the **1**-detecting parts are spread widely over the STM images.

In order to understand the observed dI/dV peaks quantitatively, a voltage distribution of W tip/vacuum/**1**/insulating layer/Au(111) surface was taken up, where insulating layer is C7S SAM. When the tunneling current flows through a molecular orbital, the positive and negative tunneling threshold voltages V_+ and V_- are expressed by eqs 1 and 2

$$V_+ = \frac{C_1 + C_2}{eC_2} E^+_{dis} \quad (1)$$

and

$$V_- = -\frac{C_1 + C_2}{eC_2} E^-_{dis} \quad (2)$$

where C_1 is the capacitance of the vacuum layer between the W tip and **1** and C_2 is the capacitance between **1** and Au(111) surface. Here, E^+_{dis} and E^-_{dis} express the energy differences between LUMO of **1** and Fermi level (E_F) and between E_F and HOMO (or HOMO−1) of **1**, respectively.[37−39] Using the electrical image method,[40−42] C_1 and C_2 were estimated to be 0.11 and 0.23 aF, respectively, provided that the relative permittivity of alkanethiol SAM is 2.6,[31,43] the distance between the W tip and **1** is 0.35 nm,[23] and the C7S SAM height above the Au(111) surface is 1.09 nm.[44]

Considering the electron donating properties of **1**,[28] the dI/dV peak at V = −1.3 V in Figure 5b is attributed to the HOMO level (E_{HOMO}) of **1**. Energy difference E^-_{dis} (= $E_F - E_{HOMO}$) is evaluated to be 0.88 eV by eq 2. As the second peak at V = −2.1 V in Figure 5b is attributed to the HOMO−1 level (E_{HOMO-1}) of **1**, the energy difference E^-_{dis} (= $E_F - E_{HOMO-1}$) is evaluated to be 1.42 eV. As a result, $E_{HOMO} - E_{HOMO-1}$ is estimated as 0.54 eV.

On the other hand, the dI/dV peak at V = 2.4 V in Figure 5b is attributed to the LUMO level (E_{LUMO}) of **1**. Energy difference E^+_{dis} (= $E_{LUMO} - E_F$) is evaluated to be 1.62 eV by eq 1. Consequently, the HOMO−LUMO gap is evaluated as 2.5 eV from the STS measurements. Therefore, the energy diagram of W tip/vacuum/**1**:C7S SAM/Au(111) structure is described as shown in Figure 6.

Here, we reconsider the STM images in Figure 2. Considering the energy levels of the molecular orbital of **1**, the observed peaks in the dI/dV spectrum at −2.1 and −1.3 V can be assigned to the E_{HOMO-1} and E_{HOMO} of **1** embedded in C7S SAM, respectively. This assignment leads to the conclusion that HOMO−1 contributes to STM images at $V < -2.1$ V and HOMO contributes to those at $-2.1 < V < -1.3$ V. In accord with this assignment, the Kohn−Sham orbital of HOMO−1 has a circle shape with more density at the center and that of HOMO has a triangular shape as shown in Figure 3.

dx.doi.org/10.1021/ja404512w | J. Am. Chem. Soc. 2013, 135, 14159−14166

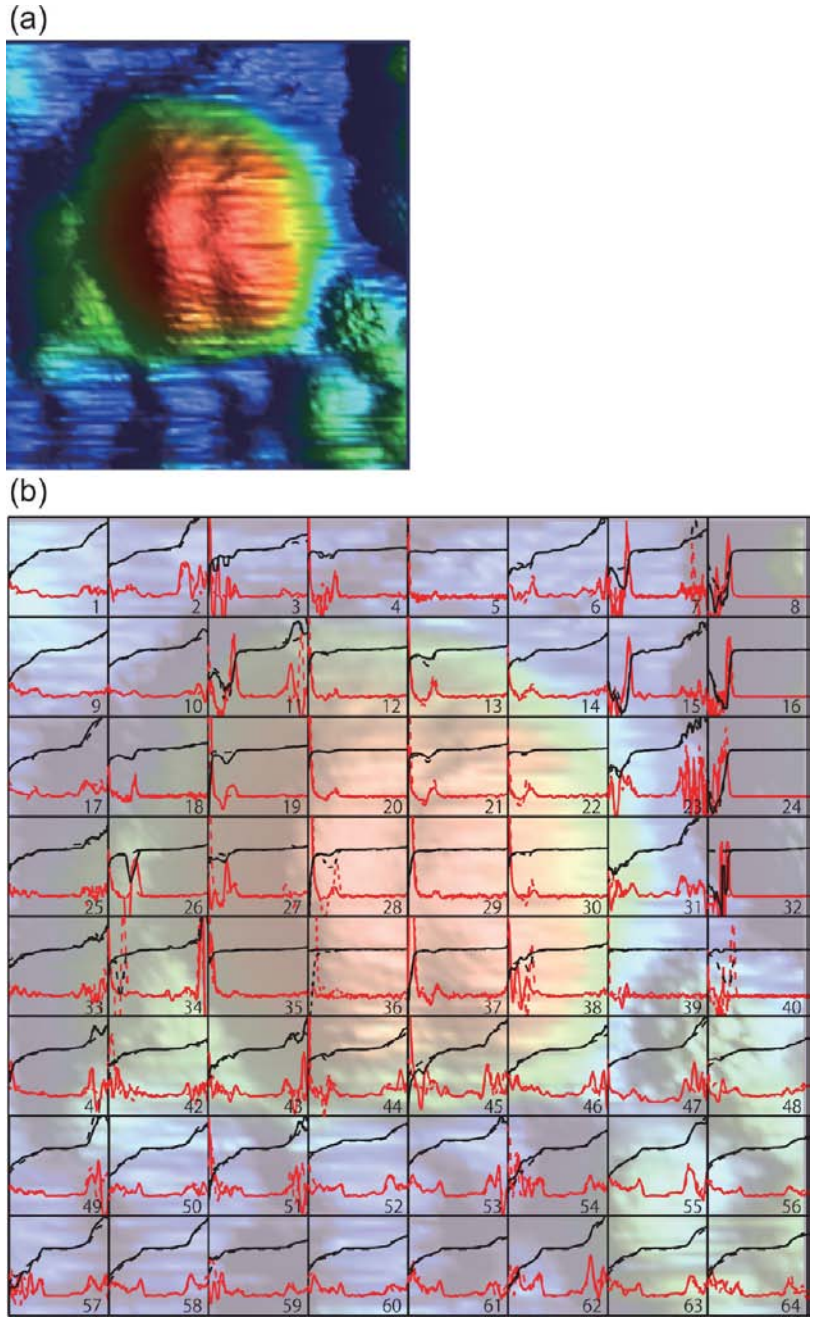

Figure 7. (a) STM image of B-pentanethioloxy tribenzosubporphine inserted in C7S SAM by tribenzosubporphine-cation attached W tip with 3 × 3 nm^2 at the sample bias voltage of −3.0 V and a set point current of −5 pA. (b) Spatial mapping of current−voltage (I−V, black lines) and differential conductance-voltage ($dI/dV - V$, red lines) characteristics at all the 8 × 8 divided parts of the STM image with consecutive bidirectional sample bias voltage sweeps from −2.5 to 2.5 V (solid line) and from 2.5 to −2.5 V (dashed line). The STM image of (a) is overlaid.

During the STM measurements, we found that the tribenzosubporphine cation was often liberated from a 5-mercaptopentoxy anchor and adsorbed on to the W tip. Figure 7a shows such a typical STM image at a sample bias voltage of −3.0 V and a set point current of −5 pA. In this case, a liberated tribenzosubporphine cation (Figure 1b) was thought to be adsorbed on to the W tip on the basis of the following observations. We found that the cation adsorbed W tip was very robust and thus once the cation was adsorbed it was rather difficult to detach the cation from the tip. Differential conductance measurements were performed on all the 8 × 8 divided parts as the same measurement conditions used to record Figure 4b and are overlaid in Figure 7b. Differently from the measurements using a bare W tip, characteristic dI/dV peaks were observed by differential conductance measurements at parts with no contribution of **1** especially at bottom-line and top-left parts in Figure 7b. As a typical example, the differential conductance measurement at part 62 was shown in Figure 8a, where discrete dI/dV main peaks are observed at V = 2.4, 1.8, −0.9, and −2.0 V. If the electroactive subporphine cation is adsorbed at the tip, the capacitance C_1' of the vacuum layer between the W tip and tribenzosubporphine cation becomes larger than that C_2' between tribenzosubporphine cation and Au(111) surface. As a result, eqs 1 and 2 are re-expressed as

dx.doi.org/10.1021/ja404512w | J. Am. Chem. Soc. 2013, 135, 14159−14166

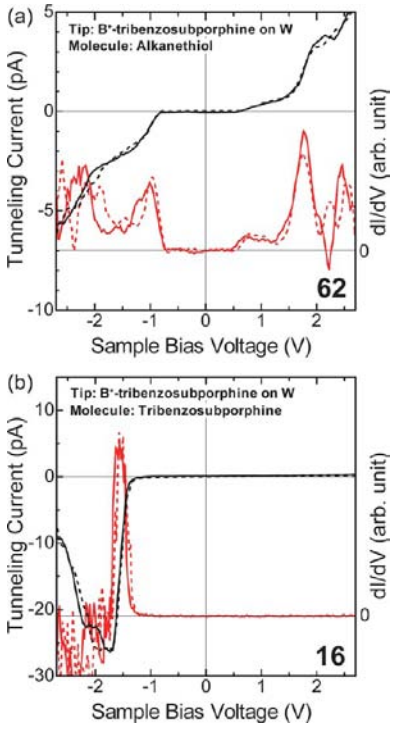

Figure 8. Representative $I-V$ and $dI/dV - V$ characteristics measured on (a) C7S SAM and (b) B-pentanethioloxy tribenzosubporphine with tribenzosubporphine-cation attached W tip, which correspond the parts 62 and 16 of Figure 7b, respectively.

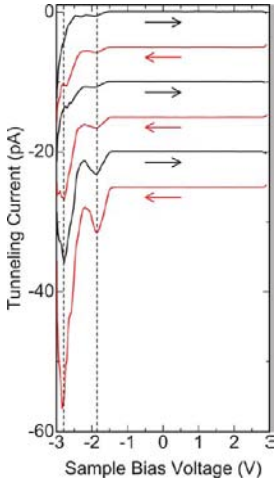

Figure 9. Consecutive bidirectional $I-V$ characteristics within a sample bias voltage range between −3 and 3 V in W tip/tribenzosubporphine-cation/vacuum/B-pentanethioloxy tribenzosubporphine:C7S mixed SAM/Au(111). Each curve has 5 pA offset in order to clarify.

$$V_+' = \frac{C_1' + C_2'}{eC_1} E_{\mathrm{dis}}^{+'} \tag{3}$$

and

$$V_-' = -\frac{C_1' + C_2'}{eC_1} E_{\mathrm{dis}}^{-'} \tag{4}$$

where, $E_{\mathrm{dis}}^{+'}$ and $E_{\mathrm{dis}}^{-'}$ express the energy differences between E_F and HOMO (or HOMO−1) of tribenzosubporphine cation and between LUMO of tribenzosubporphine cation and E_F,

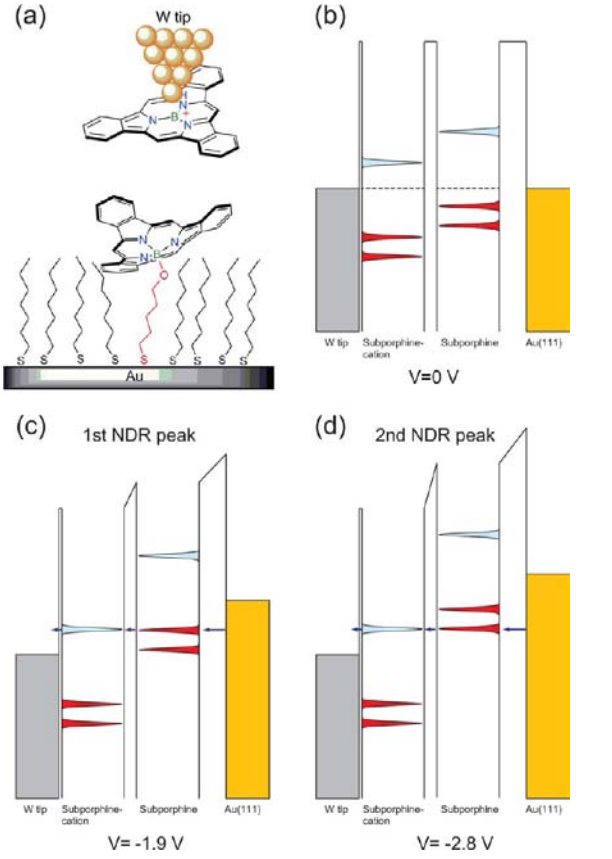

Figure 10. (a) Schematic side view and Energy diagrams of W tip/tribenzosubporphine-cation/vacuum/B-pentanethioloxy tribenzosubporphine:C7S mixed SAM/Au(111) structure at (b) V = 0, (c) −1.9, and (d) −2.8V.

respectively. Consequently, dI/dV main peaks at V = 2.4, 1.8, −0.9 are attributed to HOMO−1, HOMO, and LUMO levels. It notes that the peak voltage differences between HOMO−1 and HOMO, and between HOMO and LUMO are 0.6 and 2.7 V, respectively, which values are almost equal to the energy differences of $E_{\mathrm{HOMO}} - E_{\mathrm{HOMO-1}}$ of 0.54 eV and HOMO−LUMO gap of 2.5 eV, respectively. As a result, C_1' is much larger than C_2' ($C_1' \gg C_2'$), and the HOMO−1, HOMO, and LUMO levels of tribenzosubporphine cation are pinned to Fermi level of the W tip. It is also important to point out that the attachment of tribenzosubporphine cation can be easily confirmed by STS measurement at focusing the tribenzosubporphine-free alkanethiol area, which led to the characteristic responses similar to those shown in Figure 8a.

Energy differences $E_F - E_{\mathrm{HOMO}}$, $E_F - E_{\mathrm{HOMO-1}}$, and $E_{\mathrm{LUMO}} - E_F$ are evaluated to be 1.8, 2.4, and 0.9 eV, respectively. It notes that the HOMO−1, HOMO, and LUMO levels are approximately 0.9 eV shifted owing to the adsorbed the electroactive subporphine cation. The tribenzosubporphine cation is an electron-deficient species and its molecular orbital energies have been calculated to be stabilized by ca. 3.6 eV as shown in Figure S1 (Supporting Information).[45] Consequently, LUMO, HOMO, and HOMO−1 levels of subporphyrin cation are pinned by the W tip due to the adsorption, and are shifted 0.9 eV as compared with those of neutral subporphyrin.

As the STM image of **1** was observed in Figure 7a, differentiation of tribenzosubporphine-cation-absorbed W tip from the bare W tip is possible. Figure 8b shows the typical $I-$

dx.doi.org/10.1021/ja404512w | J. Am. Chem. Soc. 2013, 135, 14159−14166

V and $dI/dV - V$ characteristics recorded at part 16, which exhibits distinct NDR with a peak-to-valley (PV) ratio of 2.6 in both forward and backward voltage sweeps. The characteristic NDR are clearly observed at positions of 8, 16, 24, and 32. Here, the spatial ambiguity can be the STM tip drift during the STS mapping measurements. We would like to also propose that the tilting of a neutral tribenzosubporphine anchored to the metal surface, which leads to the formal expansion of STS active area over the STM image. When this tilted tribenzosubporphines is interacted with the cation-adsorbed tip, the PV ratio would depend on the molecular position but the NDR observation would be possible if there are the overlap between **1** and tribenzosubporphine-cation-absorbed W tip. These NDRs were repeatedly observed not only at $V = -1.9$ V but also at $V = -2.8$ V with consecutive bidirectional sample voltage sweep from −3 to 3 V (black line) and from 3 to −3 (red line) as shown in Figure 9.

Here, we discuss on the mechanism of the NDR phenomena based on molecular resonant tunneling. It is known that B-alkoxy subporphyrins undergo S_N1 type heterolysis to give corresponding cationic states under acidic conditions.[45] Subporphyrin cations have been shown to be planar and the corresponding tribenzosubporphine cation was indicated to be also planar by DFT calculation.[45] Energy difference between E_{LUMO} and E_F of the subporphyrin cations is 0.9 eV, and that between E_F and E_{HOMO} is 1.8 eV . These results indicate that Fermi energy of the W tip absorbing subporphyrin cations is 0.9 eV close to LUMO level rather than LUMO level of **1**. An energy diagram of W tip/tribenzosubporphirine cation/vacuum/**1**/C7S SAM/Au(111) is shown Figure 10a.

When negative sample voltage was applied to Au(111) substrate and reached at $V = -1.9$ V, an energy level alignment between the HOMO level of **1** and the LUMO level of the tribenzosubporphirine cation resulted in molecular resonant tunneling, and electrons were easy to tunnel between W tip and Au(111) through the HOMO level of **1** and the LUMO level of the tribenzosubporphirine cation. If larger negative sample bias voltage of −1.9 V was applied, the energy level overlap between the HOMO level of **1** and the LUMO level of tribenzosubporphirine cation was reduced, which resulted in a reduction in current. As a result, the first NDR with the peak and the valley was observed. More larger negative sample bias voltage was applied up to −2.8 V, the energy level overlap between the HOMO−1 level of **1** and the LUMO level of the tribenzosubporphirine cation increased again, which allowed for a second molecular resonant tunneling event. As a result, the NDR was observed. If the HOMO and HOMO−1 energy levels were close, this NDR with the PV ratio of 2.6 would not be observed since the continuous energy state prevented a conductance reduction. Therefore, it is concluded that the isolated energy levels of **1** play crucial roles in the NDR phenomena.

CONCLUDING REMARKS

In summary, the STS measurements of tribenzosubporphine **1** anchored to the Au(111) surface via a 5-mercaptopentoxy chain but embedded in the heptanethiol SAM (C7S SAM) were performed with bare W tip or a tribenzosubporphines-cation-adsorbed W tip. The method allowed us to probe the inherent electronic properties of **1**, recording a triangular shape for the HOMO and a circular shape for the HOMO−1 by molecular-resolution STM images, and evaluating the HOMO−LUMO gap to be 2.5 eV. In the spatial mapping STM, a tribzenzosubporphine cation part of **1** was often found to be liberated from the 5-mercaptopentoxy anchor and adsorbed on to the W tip. When the STS of **1** in C7S SAM was measured by using the cation-adsorbed W tip, NDR phenomena were repeatedly observed with a peak-to-valley ratio of 2.6. The observed NDR phenomena have been attributed to the molecular resonant tunneling diode operation in which the electrons tunnel between the W tip and Au(111) surface through discrete frontier molecular orbitals of **1** and its cation. Through this study, the potential of tribenzosubporphines in molecular electronic devices has been underlined in terms of compact aromatic property with discrete frontier molecular orbitals, smoothly curved molecular shape, and availability of the axial group as an anchor that allows their fixation and electronic decoupling from the metal surface through the use of SAM coated surface.

ASSOCIATED CONTENT

Supporting Information

Supplemental figure and complete ref . This material is available free of charge via the Internet at http://pubs.acs.org.

AUTHOR INFORMATION

Corresponding Authors

majima@msl.titech.ac.jp
osuka@kuchem.kyoto-u.ac.jp

Notes

The authors declare no competing financial interest.

ACKNOWLEDGMENTS

The work at Tokyo Tech was partially supported by a Grant-in-Aid for Scientific Research on Innovative Areas (No. 20108011, π - Space) from the Ministry of Education, Culture, Sports, Science and Technology (MEXT); MEXT Elements Strategy Initiative to Form Core Research Center; and the World Class University (WCU) program through the Ministry of Education, Science and Technology of Korea (R31-10022). The work at Kyoto Univ. was supported by Grants-in-Aid for Scientific Research (No. 22245006 (A)) and Grant-in-Aid for Scientific Research on Innovative Areas (No. 20108001, π - Space).

REFERENCES

(1) Tour, J. M. *Acc. Chem. Res.* **2000**, *33*, 791.
(2) Joachim, C.; Gimzewski, J.; Aviram, A. *Nature* **2000**, *408*, 541.
(3) Lu, W.; Lieber, C. M. *Nat. Mater.* **2007**, *6*, 841.
(4) Tao, N. J. *Nat. Nanotechnol.* **2006**, *1*, 173.
(5) McCreery, R. L. *Chem. Mater.* **2004**, *16*, 4477.
(6) Mantooth, B.; Weiss, P. *Proc. IEEE* **2003**, *91*, 1785.
(7) Joachim, C.; Ratner, M. *Proc. Natl. Acad. Sci. U.S.A.* **2005**, *102*, 8801.
(8) Chen, J.; Reed, M. *Chem. Phys.* **2002**, *281*, 127.
(9) Ho, W. *J. Chem. Phys.* **2002**, *117*, 11033.
(10) Hou, J. G.; Zhao, A. *Nano* **2006**, *1*, 15.
(11) Donhauser, Z.; Mantooth, B.; Kelly, K.; Bumm, L.; Monnell, J.; Stapleton, J.; Price, D.; Rawlett, A.; Allara, D.; Tour, J.; Weiss, P. *Science* **2001**, *292*, 2303.
(12) Cornil, J.; Karzazi, Y.; Brédas, J. L. *J. Am. Chem. Soc.* **2002**, *124*, 3516.
(13) Fan, F.; Lai, R.; Cornil, J.; Karzazi, Y.; Bredas, J.; Cai, L.; Cheng, L.; Yao, Y.; Price, D.; Dirk, S.; Tour, J.; Bard, A. *J. Am. Chem. Soc.* **2004**, *126*, 2568.
(14) Khondaker, S. I.; Yao, Z.; Cheng, L.; Henderson, J. C.; Yao, Y.; Tour, J. M. *Appl. Phys. Lett.* **2004**, *85*, 645.

(15) Kim, S.; Kim, B.; Park, J.; Shin, H.; Kwon, Y. *Curr. Appl. Phys.* **2006**, *6*, 608.
(16) Moore, A. M.; Dameron, A. A.; Mantooth, B. A.; Smith, R. K.; Fuchs, D. J.; Ciszek, J. W.; Maya, F.; Yao, Y.; Tour, J. M.; Weiss, P. S. *J. Am. Chem. Soc.* **2006**, *128*, 1959.
(17) Walzer, K.; Marx, E.; Greenham, N. C.; Less, R. J.; Raithby, P. R.; Stokbro, K. *J. Am. Chem. Soc.* **2004**, *126*, 1229.
(18) Xiao, X.; Nagahara, L. A.; Rawlett, A. M.; Tao, N. *J. Am. Chem. Soc.* **2005**, *127*, 9235.
(19) Karzazi, Y.; Cornil, J.; Brdas, J. L. *Nanotechnology* **2003**, *14*, 165.
(20) Zeng, C.; Wang, H.; Wang, B.; Yang, J.; Hou, J. G. *Appl. Phys. Lett.* **2000**, *77*, 3595.
(21) Hasobe, T.; Hattori, S.; Kamat, P. V.; Wada, Y.; Fukuzumi, S. *J. Mater. Chem.* **2005**, *15*, 372. T.
(22) Danilov, A. V.; Kubatkin, S. E.; Kafanov, S. G.; Bjørnholm. *Faraday Discuss.* **2006**, *131*, 337.
(23) Yasutake, Y.; Shi, Z.; Okazaki, T.; Shinohara, H.; Majima, Y. *Nano Lett.* **2005**, *5*, 1057.
(24) Liljeroth, P.; Repp, J.; Meyer, G. *Science* **2007**, *317*, 1203.
(25) Noguchi, Y.; Ueda, R.; Kubota, T.; Kamikado, T.; Yokoyama, S.; Nagase, T. *Thin Solid Films* **2008**, *516*, 2762.
(26) Wang, Y.; Kroger, J.; Berndt, R.; Hofer, W. A. *J. Am. Chem. Soc.* **2009**, *131*, 3639.
(27) Kluksdahl, N. C.; Kriman, A. M.; Ferry, D. K. *Phys. Rev. B* **1989**, *39*, 7720.
(28) Inokuma, Y.; Kwon, J. H.; Ahn, T. K.; Yoon, M.-C.; Kim, D.; Osuka, A. *Angew. Chem., Int. Ed.* **2006**, *45*, 961.
(29) Inokuma, Y.; Osuka, A. *Dalton Trans.* **2008**, *19*, 2517.
(30) Osuka, A.; Tsurumaki, E.; Tanaka, T. *Bull. Chem. Soc. Jpn.* **2012**, *84*, 679.
(31) Zhang, H.; Yasutake, Y.; Shichibu, Y.; Teranishi, T.; Majima, Y. *Phys. Rev. B* **2005**, *72*, 205441.
(32) Kohn, W.; Sham, L. J. *Phys. Rev.* **1965**, *140*, A1133.
(33) Parr, R. G.; Yang, W. *Density-Functional Theory of Atoms and Molecules*; Oxford Science: Oxford, 1994.
(34) Becke, A. D. *J. Chem. Phys.* **1993**, *98*, 5648.
(35) Lee, C.; Yang, W.; Parr, R. G. *Phys. Rev. B.* **1988**, *37*, 785.
(36) Frisch, M. J.; Trucks, G. W.; Schlegel, H. B.; Scuseria, G. E.; Robb, M. A.; Cheeseman, J. R.; Scalmani, G.; Barone, V.; Mennucci, B.; Petersson, G. A.; Nakatsuji, H.; Caricato, M.; Li, X.; Hratchian, H. P.; Izmaylov, A. F.; Bloino, J.; Zheng, G.; Sonnenberg, J. L.; Hada, M.; Ehara, M.; Toyota, K.; Fukuda, R.; Hasegawa, J.; Ishida, M.; Nakajima, T.; Honda, Y.; Kitao, O.; Nakai, H.; Vreven, T.; Montgomery, J. A.; Peralta, Jr., J. E.; Ogliaro, F.; Bearpark, M.; Heyd, J. J.; Brothers, E.; Kudin, K. N.; Staroverov, V. N.; Kobayashi, R.; Normand, J.; Raghavachari, K.; Rendell, A.; Burant, J. C.; Iyengar, S. S.; Tomasi, J.; Cossi, M.; Rega, N.; Millam, J. M.; Klene, M.; Knox, J. E.; Cross, J. B.; Bakken, V.; Adamo, C.; Jaramillo, J.; Gomperts, R.; Stratmann, R. E.; Yazyev, O.; Austin, A. J.; Cammi, R.; Pomelli, C.; Ochterski, J. W.; Martin, R. L.; Morokuma, K.; Zakrzewski, V. G.; Voth, G. A.; Salvador, P.; Dannenberg, J. J.; Dapprich, S.; Daniels, A. D.; Farkas, O.; Foresman, J. B.; Ortiz, J. V.; Cioslowski, J.; Fox, D. J. *Gaussian 09*, Revision A.02; Gaussian, Inc.: Wallingford, CT, 2009.
(37) Iwamoto, M.; Ogawa, D.; Yasutake, Y.; Azuma, Y.; Umemoto, H.; Ohashi, K.; Izumi, N.; Shinohara, H.; Majima, Y. *J. Phys. Chem. C* **2010**, *114*, 14704.
(38) Li, B.; Zeng, C.; Zhao, J.; Yang, J.; Hou, J. G.; Zhu, Q. *J. Chem. Phys.* **2006**, *124*, 064709.
(39) Zhao, J.; Zeng, C.; Cheng, X.; Wang, K.; Wang, G.; Yang, J.; Hou, J. G.; Zhu, Q. *Phys. Rev. Lett.* **2005**, *95*, 045502.
(40) Hanna, A. E.; Tinkham, M. *Phys. Rev. B* **1991**, *44*, 5919.
(41) Averin, D. V.; Likharev, K. K. In *Mesoscopic Phenomena in Solids*; Al'tshuler, B., Lee, P., Webb, R., Eds.; Elsevier: Amsterdam, 1991.
(42) Oyama, Y.; Majima, Y.; Iwamoto, M. *J. App. Phys.* **1999**, *86*, 7087.
(43) Porter, M. D.; Bright, T. B.; Allara, D. L.; Chidsey, C. E. D. *J. Am. Chem. Soc.* **1987**, *109*, 3559.
(44) Bumm, L. A.; Arnold, J. J.; Dunbar, T. D.; Allara, D. L.; Weiss, P. S. *J. Phys. Chem. B* **1999**, *103*, 8122.
(45) Tsurumaki, E.; Hayashi, S.; Tham, F. S.; Reed, C. A.; Osuka, A. *J. Am. Chem. Soc.* **2011**, *133*, 11956.